Partial Repowering Analysis of a Commercial-Scale Wind Farm by Turbine Hub Height Variation to Mitigate Upstream Wind Farms Wake Interference

By

Abdul Haseeb Syed
Reg # 00000204002
Session 2017-2019

Supervised by
Dr. Adeel Javed

A Thesis Submitted to the US Pakistan Centre for Advanced Studies in Energy in partial fulfillment of the requirements of the degree of

MASTER of SCIENCE
in
THERMAL ENERGY ENGINEERING

US-Pakistan Centre for Advanced Studies in Energy
(USPCAS-E)
National University of Sciences and Technology (NUST) H-12,
Islamabad 44000, Pakistan

December 2019

THESIS ACCEPTANCE CERTIFICATE

Certified that final copy of MS thesis written by Abdul Haseeb Syed (Registration No. 00000204002), of U.S.-Pakistan Centre for Advanced Studies in Energy has been vetted by undersigned, found complete in all respects as per NUST Statues/Regulations, is within the similarity indices limit and accepted as partial fulfillment for the award of MS/MPhil degree. It is further certified that necessary amendments as pointed out by GEC members of the scholar have also been incorporated in the said thesis.

Signature: _____

Name of Supervisor: Dr. Adeel Javed

Date: _____

Signature (HOD): _____

Date: _____

Signature (Dean/Principal): _____

Date: _____

Certificate

This is to certify that work in this thesis has been carried out by **Mr. Abdul Haseeb Syed** and completed under my supervision in, US-Pakistan Center for Advanced Studies in Energy (USPCAS-E), National University of Sciences and Technology, H-12, Islamabad, Pakistan.

Supervisor: **_____**

Dr. Adeel Javed
USPCAS-E
NUST, Islamabad

GEC member # 1:   **_____**

Dr. Adeel Waqas
USPCAS-E
NUST, Islamabad

GEC member # 2:   **_____**

Dr. Majid Ali
USPCAS-E
NUST, Islamabad

GEC member # 3:   **_____**

Dr. Ammar Mushtaq
RCMS
NUST, Islamabad

HOD-Thermal Energy Engineering: **_____**

Dr. Adeel Javed
USPCAS-E
NUST, Islamabad

Principal/ Dean: **_____**

Dr. Adeel Waqas
USPCAS-E
NUST, Islamabad

Acknowledgments

Abstract

Repowering enhances the power generation capacity and service life of wind farms. In this study, a partial repowering strategy has been analyzed for a large commercial-scale wind farm in Jhimpir, Pakistan. The wind farm is highly influenced by upstream farms wake interference. Wind speed and power deficit of individual turbines were evaluated using the mesoscale Weather Research and Forecasting (WRF) model coupled with Wind Farm Parameterization scheme. The test case wind farm is experiencing a 15% reduction in wind speed and 35% decline in power production due to the presence of upstream farms. The wind speed and power results from the WRF model were also validated by comparison with the observed data. Wind turbines with the highest power deficit were identified and their hub heights were varied to mitigate the wake interaction. Wind shear profiles and power output of modified turbines were evaluated at the new hub height of 61.5m and 100m separately and compared with the existing hub height of 80m. A power reduction of up to 12% was observed in the 61.5m hub height case, while an increase of up to 13.6% was seen in the 100m hub height case compared to the existing layout. A mean increase of 4.9% was observed in the total power generation of the modified wind farm which can lead to a significant increase in annual energy production. This research work lays out the foundation for repowering of old wind farms in Pakistan and around the world, as it presents the use of mesoscale model as a fast and reliable tool for technical assessment of old wind farms.

Keywords: Wind farm; repowering; mesoscale simulation; wake interference; hub height variation; model validation

Table of Contents

List of Figures

List of Tables

Nomenclature

Variables		Abbreviations	
A	Rotor Area	AEP	Annual Energy Production
C_P	Power Coefficient	AGL	Above Ground Level
C_T	Thrust Coefficient	ARW	Advanced Research WRF
C_{TKE}	TKE Coefficient	CFD	Computational Fluid Dynamics
D	Rotor Diameter	DIBt	German Institute for Construction Technology
F_D	Drag Force	GFS	Global Forecast System
H	Height	IA	Index of Agreement
H_{hub}	Hub Height	IEC	International Electrotechnical Commission
P_{rated}	Rated Power	KE	Kinetic Energy
P	Pressure	LES	Large Eddy Simulation
V	Horizontal Wind Speed	MABE	Mean Absolute Bias Error
V_{rated}	Rated velocity	MAPE	Mean Absolute Percentage Error
Δx, Δy	Grid size in horizontal direction	MODIS	Moderate Resolution Imaging Spectroradiometer
Δz	Grid size in vertical direction	NCEP	National Centers for Environmental Prediction
η	Vertical coordinate	NWP	Numerical Weather Prediction
ρ	Air Density	R	Pearson Correlation coefficient
		RMSE	Root Mean Square Error
		RRMSE	Relative Root Mean Square Error
		SCADA	Supervisory Control and Data Acquisition
		TKE	Turbulent Kinetic Energy
		UTC	Coordinated Universal Time
		WRF	Weather Research and Forecasting

Chapter 1

Introduction

1.1   Motivation

Wind power generation is growing at a rapid pace with a total global capacity of 564 GW in 2018 [1]. Wind energy is one of the most sustainable energy sources in the world with minimal environmental repercussions. The cost per unit of wind energy is also declining due to the advancements in the field of wind turbines. As a result, the wind has become a more affordable and cleaner source of obtaining electricity as compared to conventional methods. As of 2018, about 95% of the world's cumulative wind power comes from onshore wind farms [1]. Most of the inland wind turbine farms are located in regions with high mean wind speeds throughout the year. Such wind farms are usually tightly packed with turbines having less inter-farm and intra-farm distances due to economical and spatial constraints. Therefore, wakes emerged from upstream wind farms, relative to the prevailing wind direction, cause a flow disruption and speed deficit for downstream farms. Modeling and evaluation of wake flow is essential for the design and development of new wind farms and repowering of existing ones.

Wind farms are either decommissioned or repowered at the end of their service life which is 20 to 25 years [2]. Repowering process consists of replacing all the turbines in a farm with new efficient ones i.e. full repowering or altering some specific turbines i.e. partial repowering. This process increases the life of existing wind power plants and allows the power companies to utilize the established wind energy sites for longer periods. A meticulous wake analysis of wind farms is required in order to evaluate the different repowering strategies.

1.2   Case Study

In Pakistan, wind energy has seen remarkable growth in the last decade as more than 1GW capacity is installed [1]. More than 70% of installed capacity lies in Jhimpir, a region which lies 120 km north of Karachi and contains more than eighteen operational wind

farms[3]. These farms not only influence the downstream wind characteristics but also affect the local atmospheric boundary layer in the region. Many of these farms will reach the end of their operational life at the end of the next decade and will require a life extension or repowering procedure to enhance the power generation from Jhimpir.

Figure 1.1 Wind Farms in Jhimpir, Pakistan

In this study, we have discussed a partial repowering strategy for a commercial-scale wind farm, operated by FFC Energy Ltd. (FFCEL) Pakistan, in Jhimpir influenced by wake flow and speed deficit from upstream wind farms. Due to close spacing between turbine rows within the farm and between two farms, wake structures emerge which are responsible for the speed and power deficit, and a substantial decline in Annual Energy Production (AEP)[4]. The mesoscale Weather Research and Forecasting (WRF) model with Wind Farm Parameterization scheme was applied to calculate the wind speed and power losses within the test case wind farm. Selected wind turbines with the highest power deficit were repowered by varying their hub heights. The effects of the proposed partial repowering process on the overall wind farm's power output are discussed.

1.3   Objectives
The research presented in this thesis was carried out to achieve the following objectives:

a. Determine wake effects on the FFCEL wind farm due to the presence of two upstream wind farms

b. Evaluate speed and power deficit for individual wind turbine generators and whole wind farm

c. Identify wind turbine generators with the highest power deficit

d. Determine the optimum hub height for affected turbines as a partial repowering strategy

Fig. 1.2 illustrates the methodology used in this study. The WRF model with wind farm parameterization needs geographic and time-dependent data as inputs apart from the wind turbines data. The model wind speed and power results were compared with the observed data of the same period before analyzing the hub height optimization approach.
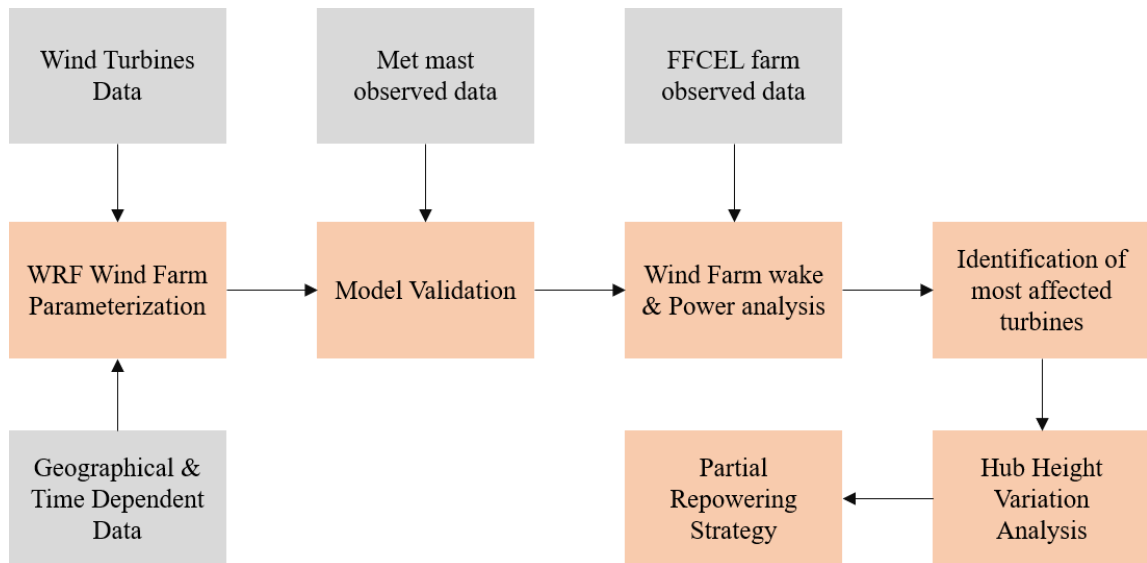
Figure 1.2 Methodology for the proposed partial repowering study of the FFCEL Wind farm

1.4 Thesis Outline

The following is a summary of the different chapters in this thesis.

Chapter 2 discusses the literature review, and different models applied by the scientific community to evaluate wake losses in wind farms. The methods discussed are Analytical models, Numerical solutions (CFD, LES), and Mesoscale models. The pros and cons of each method are discussed with their applications.

Chapter 3 describes the FFCEL and two upstream wind farm characteristics in detail. WRF model parameters applied in this study are also mentioned with the boundary and initial conditions used.

Chapter 4 includes validation of the WRF model results with observed data from the wind farm. Wind speed and direction data are quantitatively analyzed using different statistical parameters.

Chapter 5 discusses the results that emerged from the study. Wake losses and power output of the test case wind farm are analyzed. Wind turbine generators with the highest power losses are also identified using observed data from the FFCEL wind farm. This chapter also includes the hub height variation study of affected turbines. Wind speed and power output are analyzed at the new hub heights and percentage variation is observed. Wind shear profiles at the individual turbines are also presented.

Chapter 6 contains the conclusions and future research topics that are emerged from the current study.

Summary

Wind energy generation has experienced a hug surge in Pakistan over the last decade as a result of injection of more than 1 GW capacity. Many of the wind farms are located in Jhimpir, a region located in the southern province of Sindh. These wind farms are closely spaced due to land restrictions, project economics, and grid connectivity. This study deals with the wake losses occurred in a test case onshore wind farm i.e. FFCEL as a result of upstream wind farms. A brief summary of the study objectives and work presented in all the chapters is presented in Chapter 1.

Chapter 2

<div align="right">

Literature Review

</div>

2.1   Analytical Models

Simple and computationally cost-effective analytical models are often utilized to evaluate speed and power deficit in the presence of a single turbine or multiple arrays. C.L. Archer et al. [5] evaluated the performance of six famous wake models on the two offshore and one onshore wind farm located in Sweden and Denmark. The six models tested were: Jensen, Larsen, Frandsen, Bastankah and Porté-Agel, Xie and Archer, and Geometric. Among these six analytical models, Jensen, and Xie and Archer showed the best overall performance when compared with the observed data. L. Wang et al. [6] also compared three different analytical models for the power output calculations of Horns Rev offshore wind farm in Denmark and found that the accuracy of Jensen model depends on the surface roughness value, while the Larsen model showed good accuracy with the CFD results for a wind farm with variable hub height turbines. Another comparison between analytical wake models done by S. Jeon et al. [7] for an onshore wind farm suggested Jensen model be most reliable in calculating speed losses in the wake center and concluded that the accuracy of these models depends on the distance from turbine rotor. Hybrid Jensen-Gaussian analytical model [8] with more realistic results is also utilized for turbine layout studies using a genetic algorithm. Although computationally fast, analytical models underestimate wake losses because of neglecting the terrain and boundary layer effects. Some analytical models assume a linear downstream wind profile [9]–[11], while other a Gaussian profile [12]. The real-time variation within wake flow is also ignored by most analytical models, which pose questions to the accuracy of such models for turbine micro-siting or repowering purposes.

2.2   Numerical Models

Numerical models for wake flow analysis are high precision but computationally expensive due to their ability to resolve wake structures to microscale level. The majority of the numerical studies mentioned in literature only dealt with a single turbine or a

hypothetical layout of wind turbines to lower the computational cost. Numerical models like CFD and LES are often simplified by using actuator line and actuator disk methods for wind turbines flow simulation. Different wake control methods were studied by Y. Wang et al. [13] in an offshore wind farm using OpenFOAM CFD, but this study overlooked the complex wake overlapping found in large scale wind farms due to the presence of only two turbines. Large-eddy simulation (LES) modeling based on actuator line and disk methods are often utilized for resolving near wake structures. A similar study by F. Porté-Agel [14] resolved the effects of turbines on the local atmospheric boundary layer. Better correlation of LES models with observed data as compared to analytical models was also proved by X. Yang et al. [15] who studied the power output of a commercial-scale wind farm in complex terrain. Different staggered configurations, both lateral and vertical, for a large-scale wind farm were also tested by Y.-T. Wu et al. [16] using LES. Terrain and wake overlapping effects were also investigated using actuator disk models to get more accurate results [17], [18]. Simplified numerical models using Reynolds averaged Navier-Stokes equations were also employed to lower the computational cost for wind turbine wake calculations [19]. Numerical models are not suitable for studying wake interference between commercial-scale wind farms due to their significantly high computational cost.

2.3   Mesoscale Models

Wind farm repowering process requires fast and reliable solutions related to wake interference so that the effects of varying different parameters on the overall energy production can be analyzed. Mesoscale models can be the answer to the above-mentioned issues especially when resolving microscale wake structures is not the primary objective. Mesoscale weather prediction models are frequently utilized for forecasting and resource assessment applications. Z. Guo et al. [20] utilized the mesoscale Weather Research and Forecasting (WRF) model for wind resource analysis. The results obtained from the model were evaluated against the observations and probability distribution functions. In another study conducted in the North Sea[21], the WRF model results were found to have a high correlation with the recorded observations. A Wind Farm Parameterization scheme introduced by Fitch et al. [22] treated wind turbines as a drag and turbulence source creating a speed loss and gain in turbulent kinetic energy. This scheme was successfully

tested [23]at a high resolution on the Horns Rev offshore farm to analyze wake effects and power losses. Downstream effects of two inland wind farms in China were investigated[24], [25] using the WRF model integrated with the Fitch scheme at high horizontal resolutions and the results produced were in accordance with the observations. Sensitivity analysis of the WRF model by observing the effect of different resolutions, wind characteristics, and boundary layer schemes was also carried out[26], [27]. Mesoscale models like WRF are much coarser than numerical models but deliver a much faster method to analyze large scale wind farms wake effects. Such models are valuable for the design and development of farm layout, resource assessment, and the repowering process as they provide time-dependent results based on geographical and technical parameters.
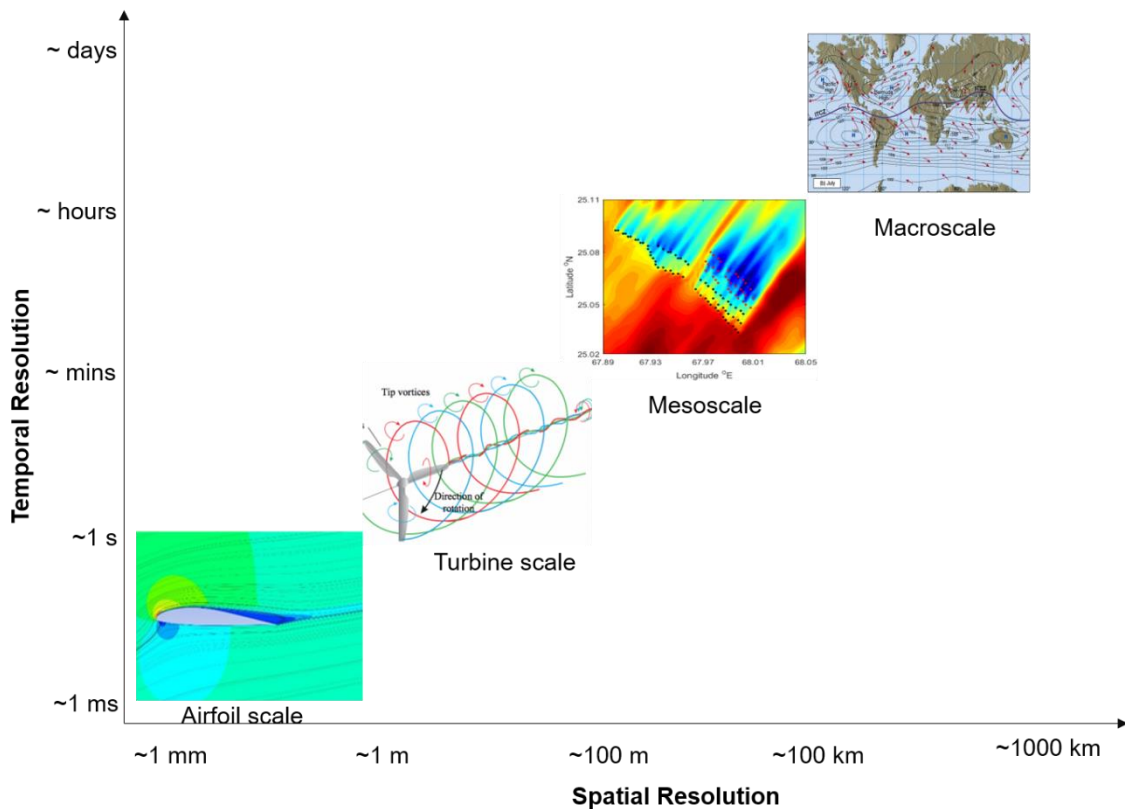
Figure 2.1 Range of scales in wind energy applications

Wind energy applications include a wide range of flow from macroscale meteorological level to microscale wind turbine blade level. The macroscale effects are mostly related to the weather and free atmosphere above the wind farms having a horizontal resolution

range of 100-1000 km. Mesoscale level combines the effects of atmospheric and wind farm scale flow; incorporating the effects of local topography, aerodynamic forces and wind turbines on the variation of atmospheric boundary layer within and outside a wind farm. The horizontal resolution of mesoscale flow spans from ~100m to ~100km. Microscale flows correspond to the interaction between a single turbine and airflow or at a much high-resolution level of an airfoil. All these complex phenomena happening at different ranges of scales contribute to the wake effects produced by a wind farm [28].

2.4   Hub Height Variation

Hub height variation within a wind farm is a suitable option to mitigate the wake effects of upstream wind farms. In this process, hub heights of certain turbines are altered to increase the overall power production. Many have reported the benefit of having different hub height turbines in a wind farm in literature. Genetic and greedy algorithms developed by Y. Chen et al.[29] and K. Chen et al.[30] respectively for layout optimization studies resulted in improved performance of a utility-scale wind farm with multiple hub heights. Multiple hub height wind turbines can lead to a decrease in turbulence and increased power generation as concluded by LES studies conducted separately by Wu et al. [16] and Archer et al. [31].

Summary

In Chapter 2, three most common wake loss estimating techniques were analyzed namely Analytical, Numerical and Mesoscale models. Analytical models, due to their fast processing speed, are most commonly used for wake prediction. Numerical CFD models although more accurate, requires immense computational power. Mesoscale models like WRF numerical weather prediction model, although relatively coarser, produce quick results of large scale wind farms wake losses based on topography and atmospheric parameters.

Chapter 3

Wind Farm Parameters and WRF Model Configuration

3.1   Wind Farm Parameters

The test case wind farm i.e. FFCEL is situated in complex terrain and influenced by the wake flow of two upstream wind farms, operated separately by Zorlu Energy Ltd. (Zorlu) And Three Gorges First Wind Farm (TGF). A high-speed sea breeze is present in Jhimpir region during the summer months flowing from the South-West direction. Fig. 3.1 represents the average monthly speeds and direction for the year 2018 in the region.

(a) Monthly Mean Wind Speeds   (b) Wind Rose Chart
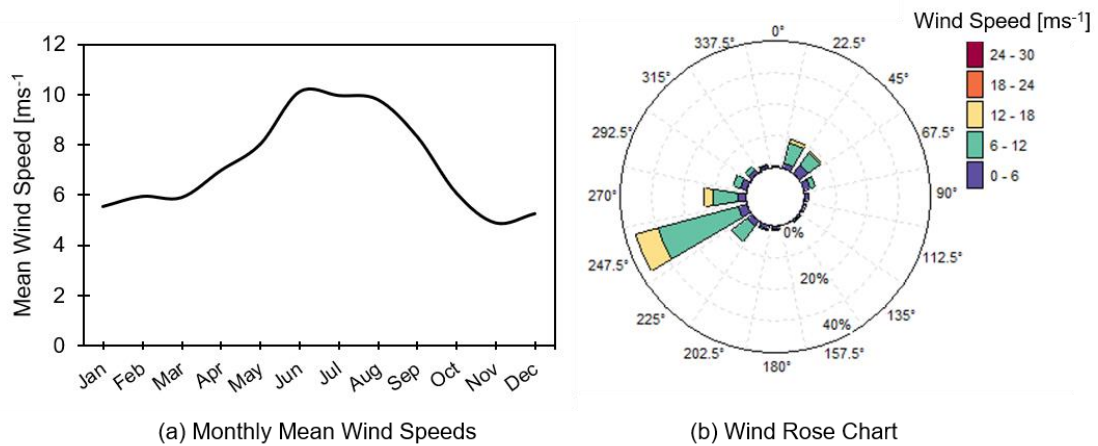
Figure 3.1 Monthly mean wind speeds and direction in Jhimpir (2018)
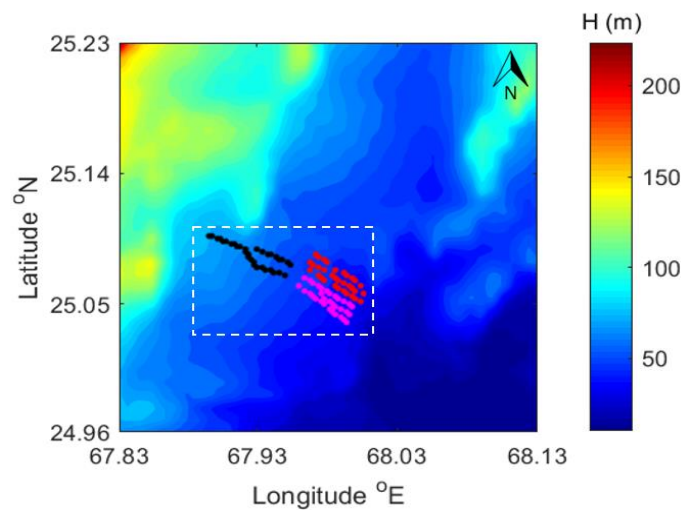
Figure 3.2 Terrain altitude of Jhimpir, Pakistan

The terrain of Jhimpir falls in a complex category with a range of local altitudes between 40m and 200m as displayed in Fig. 3.2. A schematic layout of the three wind farms in Fig. 3.3 shows less inter-farm and intra-farm spacing. Tight spacing between turbine rows leads to a substantial power loss for downstream rows due to increased turbulence. Local wind speed, direction, pressure, and air temperature data is being recorded by a met mast located in the vicinity of FFCEL. This data is used to validate the simulation results in the next chapter. Table 3.1 contains the different technical parameters related to wind farms. The manufacturer provided wind turbines data which will be used as input in the WRF model is also presented in Fig. 3.5.
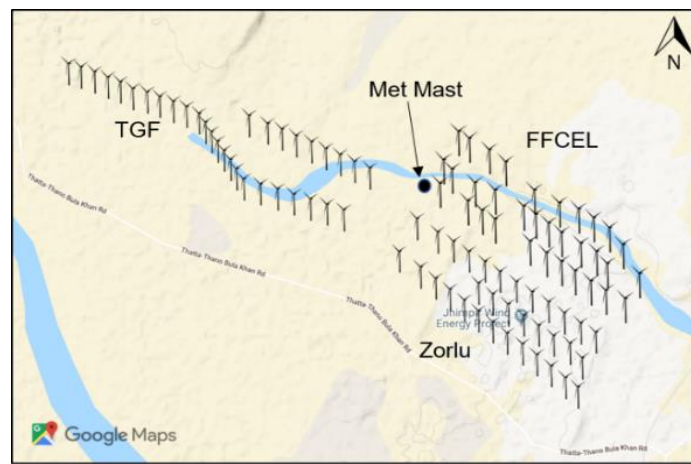
Figure 3.3 Layout of the test case and two upstream windfarms in Jhimpir, Pakistan
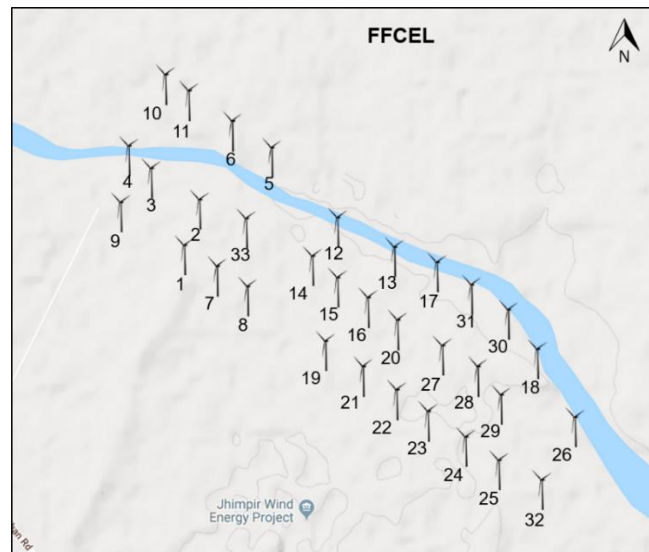
Figure 3.4 FFCEL wind farm layout

Table 3.1 Technical parameters of the wind farms

	FFCEL (Test Case)	Zorlu (Upstream)		TGF (Upstream)
Operational Date	May 2013	July 2013		November 2014
Power Capacity (MW)	49.5	56.4		49.5
No. of Turbines	33 x 1.5MW	28 x 1.8MW	5 x 1.2MW	33 x 1.5 MW
Turbines Model	Nordex S77 1.5 MW	Vestas V90 1.8 MW	Vensys V62 1.2 MW	Goldwind GW77 1.5 MW
Hub Height (m)	80	80	69	85
Rotor Diameter (m)	77	90	62	77
Spacing	Irregular	Irregular		Irregular
Inter-Farm Minimum Distance (m)	-	~790		~1390
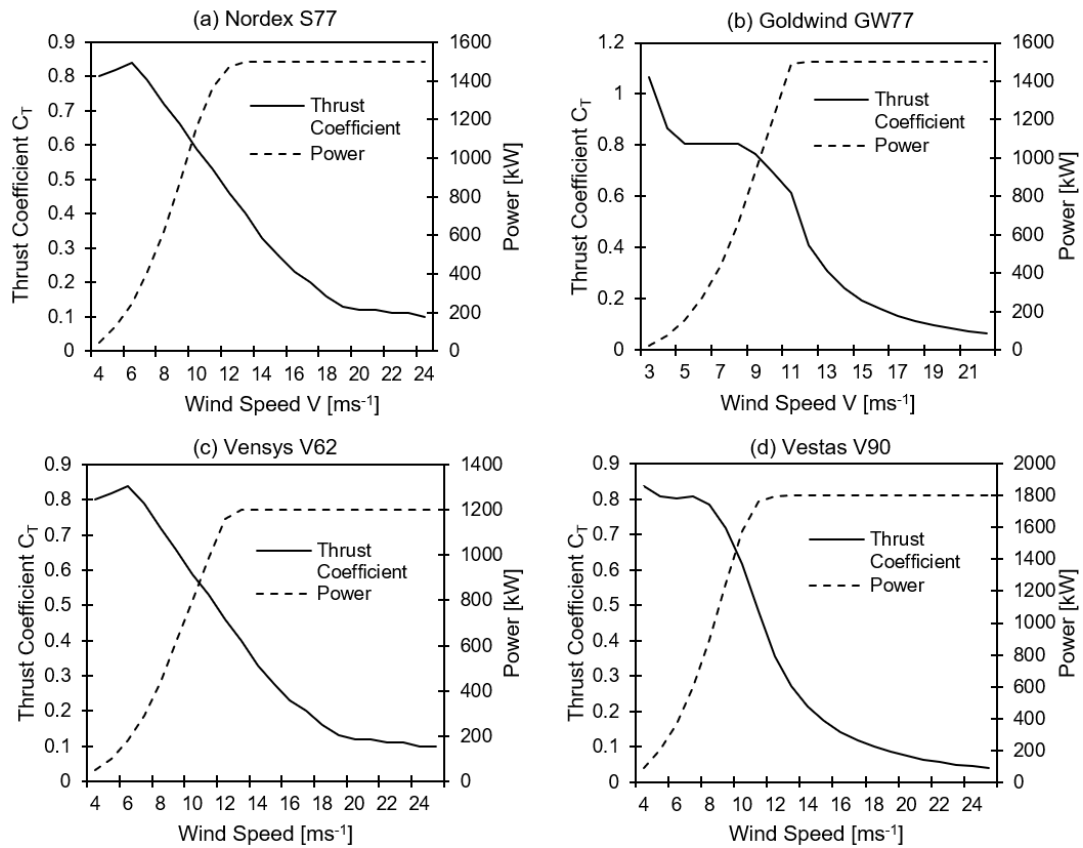
Figure 3.5 Power and thrust curves of the turbines

3.2 WRF Model Configuration

Wind Farm Parameterization scheme introduced by Fitch et al. [22] treats wind turbines as a drag source which creates a speed deficit and generates turbulence. Previously a similar scheme was introduced which utilized a constant power coefficient C_P and turbulent kinetic energy TKE value for speed deficit calculations [32]. Later improvements included using manufacturer-provided C_P values[33] and the addition of electrical and mechanical losses[34]. But the Fitch scheme introduced significant improvements to previous models as it calculates TKE from the manufacturer provided thrust curve where the value of thrust coefficient C_T is not a constant but depends on the wind speed $V(u,v)$. The value of C_T is considered as a sum of energy converted into useful energy C_P, and turbulent kinetic energy C_{TKE}.

$$C_T = C_P + C_{TKE} \qquad (3.1)$$

The drag force F_D on the turbine rotor is:

$$F_D = \frac{1}{2}.C_T(V).\rho.A.V^2 \quad (3.2)$$

Where V represents the incoming wind speed, ρ is the air density, A represents the turbine rotor area. Due to the presence of wind turbine, kinetic energy loss from the local atmosphere is:

$$\frac{\partial KE_D^{ijk}}{\partial t} = \frac{1}{2}.N_t^{ij}.\Delta x.\Delta y.C_T(V).A_{ijk}.|V|_{ijk}^3 \qquad (3.3)$$

Where cell indices are represented by i, j, k in zonal, meridional, and vertical directions respectively. Δx, Δy, and Δz indicate model resolution in three directions. ∂KE_D^{ijk} is the kinetic energy change due to drag force, N_t^{ij} indicates no. of turbines in cell i, j. Equations 3.4 and 3.5 are used to evaluate the useful power P and turbulent kinetic energy T_{TKE} in the Fitch scheme.

$$\frac{\partial P_{ijk}}{\partial t} = \frac{\frac{1}{2}.N_t^{ij}.C_P(V).A_{ijk}.|V|_{ijk}^3}{\Delta z} \qquad (3.4)$$

$$\frac{\partial \text{TKE}_{ijk}}{\partial t} = \frac{\frac{1}{2} \cdot N_t^{ij} \cdot C_{\text{TKE}}(V) \cdot A_{ijk} \cdot |V|_{ijk}^3}{\Delta z} \qquad (3.5)$$

Fitch scheme doesn't include wind turbine tower drag losses or the electrical and mechanical losses from bearings, generators, gearbox and other related components. It also assumes a wind flow perpendicular to the rotor with no effect of vertical winds on the induced drag. A schematic presentation of this scheme is shown in Fig. 3.6.
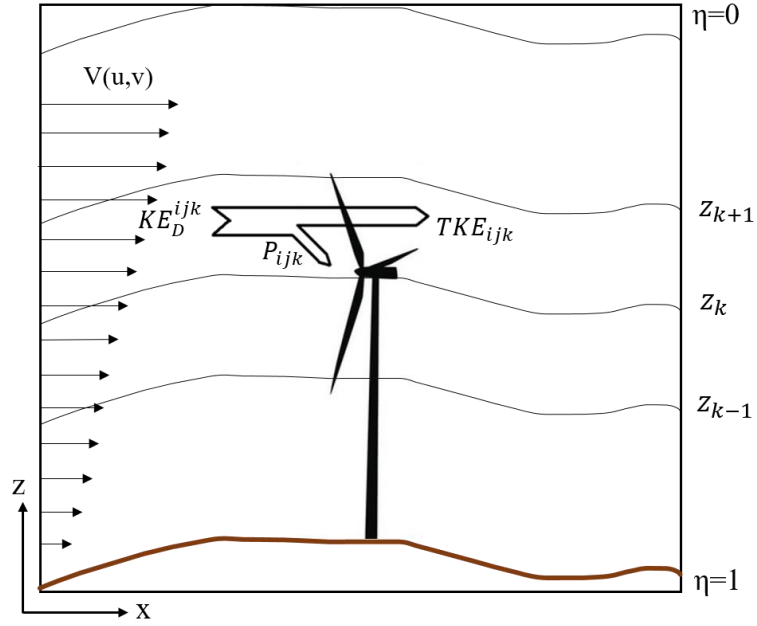
Figure 3.6 Windfarm parameterization scheme illustration

Advanced Research WRF (ARW) dynamic solver[35] uses non-hydrostatic Euler equations to evaluate parameters like pressure, precipitation, temperature and wind speed. Terrain data and time-dependent data are used as input along with turbine power and thrust curves, and geographic coordinates. Arakawa C-grid with terrain-following coordinate η calculates vector quantities like wind speed on cell faces and mass quantities like density on cell center. Terrain following coordinate η is used to eliminate the intersection of the vertical level with terrain, and can be defined as[36]:

$$\eta = \frac{P - P_t}{P_s - P_t} \qquad (3.6)$$

where P_t represents the pressure at the model top, and P_s indicates the surface pressure. Consequently, η has values of 0 and 1 at the top and surface respectively. (Fig. 3.6)
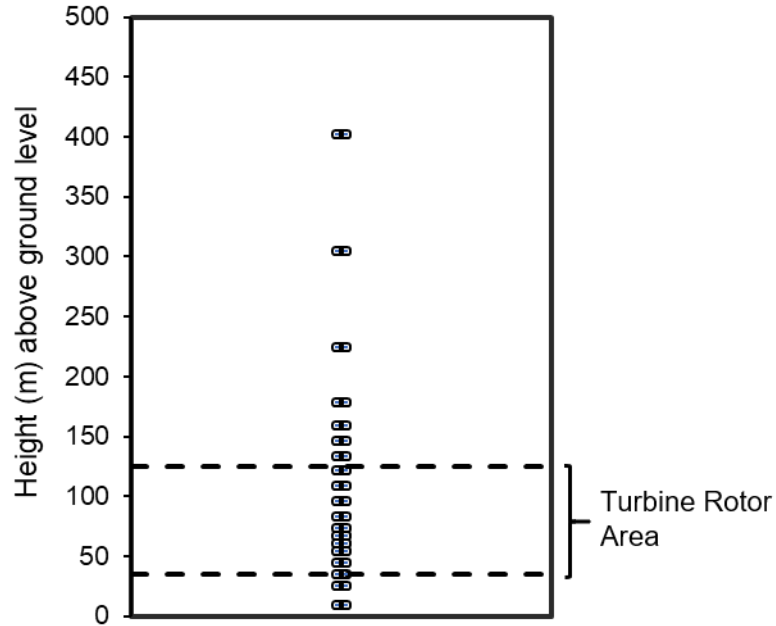
Figure 3.7 Vertical levels design

Five nested domains (Appendix A) are applied in the model where the outer domain has a resolution of 16.2 km and the innermost domain has a very high resolution of 0.2 km. 42 vertical levels are designed from the bottom where $P=P_s$ to the top where $P=30$ kPa. A high resolution is needed in the turbine rotor area, so 16 levels are kept below 200m and then remaining are geometrically stretched to the model top (Fig. 3.7). Global Forecast System (GFS) data with a resolution of 0.5 degrees is used as time-dependent data, while Moderate Resolution Imaging Spectroradiometer (MODIS) data with a resolution of 30 arc second is employed as geographical data. Two-way nesting between the domains is applied to allow feedback and analysis nudging for wind speeds and temperature is applied to the outermost coarsest domain. The planetary boundary layer scheme developed by Mellor-Yamada-Nakanishi-Niino (MYNN 2.5)[37] is employed to determine turbulent kinetic energy on the cell mass points. To identify the wake effects produced by wind farms, radiation and surface heat flux is not applied in the model. Table 3.2 describes the different model parameters used in the WRF model for simulating wind farm effects. NCAR Command Language (NCL) was used for the postprocessing of the WRF output.

The detailed code utilized for determining wind speeds and direction is mentioned in Appendix B.

Table 3.2 WRF model parameters

| WRF Model Configuration	
WRF Version	4.1
Runtime Period	01 July 2018 00hrs - 06 July 2018 00hrs
No. of domains	5
Horizontal resolution (km)	16.2, 5.4, 1.8, 0.6, 0.2
Grid points ($n_x = n_y$)	70, 94, 121, 166, 151
Vertical Levels	42
Initial Condition Data	NCEP GFS, 0.5-degree x 0.5-degree
Topographic data	MODIS 30 arc second
Nudging	Grid/ analysis nudging
Time Step	64.8 s
Nesting	Two-way nesting with feedback
Physics schemes	
Planetary Boundary Layer	MYNN 2.5 Level [37]
Microphysics	WRF Single Moment 6-class [38]
Cumulus Parameterization	Grell-Freitas [39]
Land Surface Model	Unified Noah LSM

Summary

The three test case wind farms and WRF model configuration are discussed in the Chapter 3 of this thesis. The three wind farms are located in a complex terrain where there is a strong interaction between the farms due to cloe spacing. The wind farm parameterization scheme was illustrated and discussed in detail with all the configuration parameters used in this study.

Chapter 4

WRF Model Validation

Wind speed and direction data were recorded by a met mast located just outside the FFCEL. Two mechanical cup anemometers were used to record wind speed at the hub height of 80m AGL and rotor bottom height of 41.5m. A vane at 78.5m AGL logged the wind direction observations. Both wind speed and direction data were logged as average values of a ten-minutes interval. A graphical analysis between WRF simulated wind speeds and observed values with respect to time is shown in Fig. 4.1. A 95% confidence interval of recorded data is also displayed as a colored band. Except for a few outliers, most of the simulated values are present within the confidence interval band. WRF simulated and observed wind direction data are also displayed in the form of a wind rose charts in Fig. 4.2. While the WRF simulated wind speed results are slightly underestimated, the wind direction results show high correspondence with the observed data as a dominant South-West direction can be seen in both datasets.
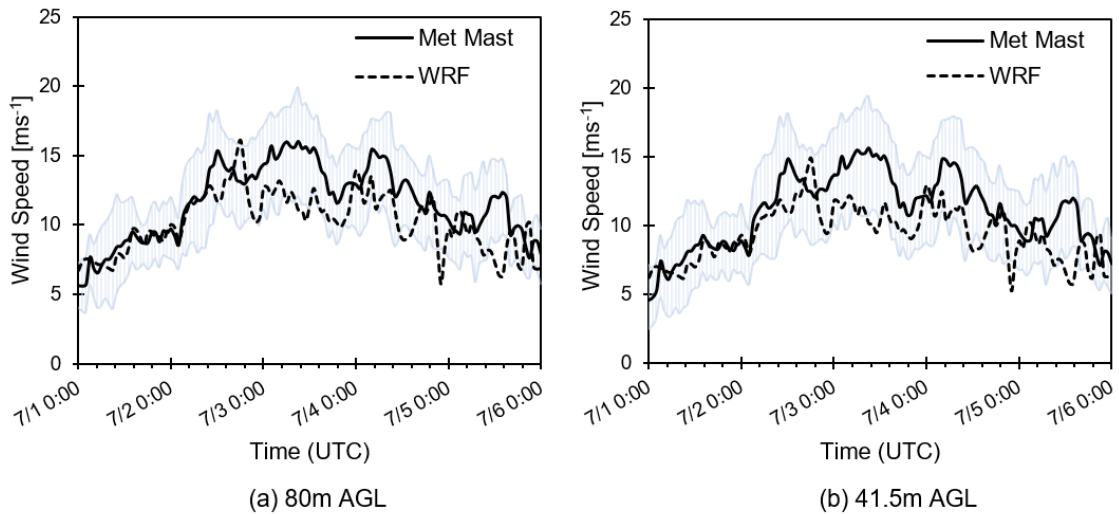
Figure 4.1 Wind speed comparison from July 1-July 5 (2018)

A quantitative analysis of WRF simulated wind speed and direction results is also performed by evaluating the following statistical parameters[21], [40]:

a. Mean Absolute Percentage Error (MAPE)

b. Mean Absolute Bias Error (MABE)

c. Root Mean Square Error (RMSE)

d. Relative Root Mean Square Error (RRMSE)

e. Pearson correlation coefficient (R)

f. Index of Agreement (IA)
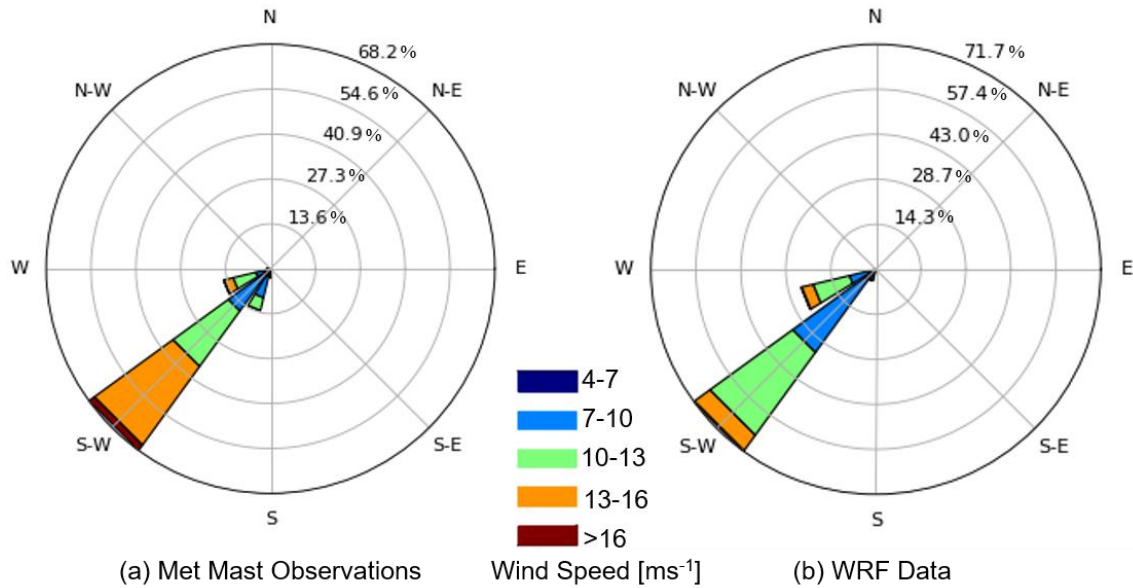
Figure 4.2 Wind direction comparison from July 1-July 5 (2018)

As observed from Table 4.1, the model's ability to predict wind speed improved with the height above ground level, due to low MAPE. The average bias between simulated and measured data also gets reduced at 80m AGL. Low variance and bias in the simulated data at higher altitudes are also indicated by RMSE and RRMSE at 80m AGL. A substantial correlation (R) is also present between the WRF simulated and met mast data. IA indicates the prediction accuracy of the WRF model, which has a high value of 0.76 at the hub height of turbines.

Table 4.1 Wind speed quantitative analysis

	MAPE (%)	MABE (ms⁻¹)	RMSE (ms⁻¹)	RRMSE	R	IA
80m AGL	14.7	1.7	2.2	0.19	0.72	0.76
41.5m AGL	17.1	1.9	2.4	0.22	0.71	0.71

Table 4.2 Wind direction quantitative analysis

	MAPE (%)	MABE (º)	RMSE (º)	RRMSE
78.5m AGL	5.5	12.25	16.08	0.07

WRF direction results showed a significant high accuracy with MAPE of only 5.5%. (Table 4.2). A low value of RRMSE shows little variance between the two datasets. Other statistical indicators also showed high accuracy of the WRF model in predicting wind direction. Concluding from the above discussion, the model can be satisfactorily used to simulate the wake interference effects between the three wind farms located in Jhimpir.

Summary

WRF model wind speed and direction results were compared with the observed data from a met mast both qualitatively and quantitatively. It was observed that WRF underestimated the wind speeds with an absolute percentage error of 14.7%. Wind direction was predicted with a very high accuracy, an absolute percentage error of only 5.5%.

5.1 Wake Interference

Two separate cases were analyzed to distinguish the flow disruption caused by Zorlu and TGF on the FFCEL wind farm. Case 1 constituted the effect of all three wind farms on the atmospheric boundary layer, while Case 2 consists of studying the effects of FFCEL only. Velocity contours of both cases are shown in Fig. 5.1 where a freestream wind speed of 12 ms^{-1} can be observed incoming from a South-West direction.

(a) Case 1 (b) Case 2
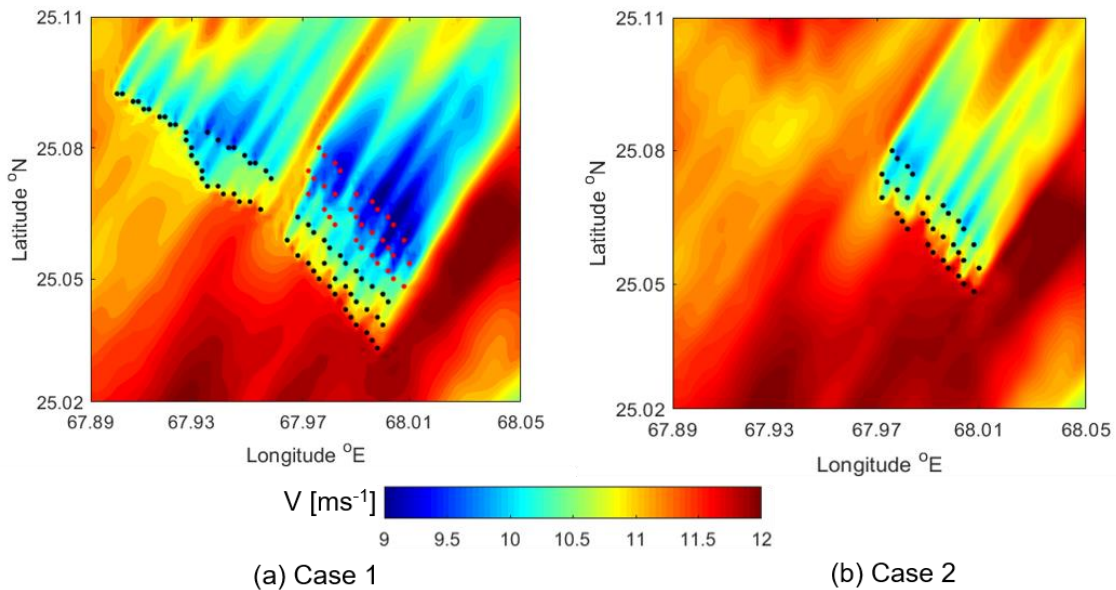
Figure 5.1 Velocity contours at H$_{hub}$=80m (a) in the presence of all three farms, and (b) only FFCEL

A substantial drop in wind speed can be observed due to the disturbance caused by upstream wind farms in Case 1. Speed deficit increases with the number of turbine rows in the direction of the prevailing wind, which can be seen in Fig. 5.1 as the last row of turbines in FFCEL has observed a velocity drop of about 3 ms^{-1} compared to the freestream speed. An inter-farm distance of 14D-16D is recommended for wind speed recovery but in this case, the first row of FFCEL did not experience the free stream

velocity due to a very less distance between FFCEL and Zorlu i.e. 9D. Due to the predominant South-West wind direction, Zorlu has more impact on FFCEL rather than TGF. Although there are some intra-farm wakes to emerge in Case 2, the wind speeds observed by FFCEL in the absence of upstream farms are much higher.

Speed deficit in percentage was also analyzed as shown in Fig. 5.2. The results showed that the first row of FFCEL in the presence of both upstream farms is experiencing the highest deficit as compared to the freestream speed. The wake effects are higher in the South-East end of the test case wind farm, due to lower altitude of terrain on that side and the half second row of turbines in the upstream wind farm. The small rotor diameter (D=77m) turbines of FFCEL are completely submerged inside the wakes imposed by larger rotor diameter turbines (D=90m) in Zorlu, adding to the turbulence and speed deficit generated.

(a) Speed deficit contours

(b) Speed deficit observed by individual turbines
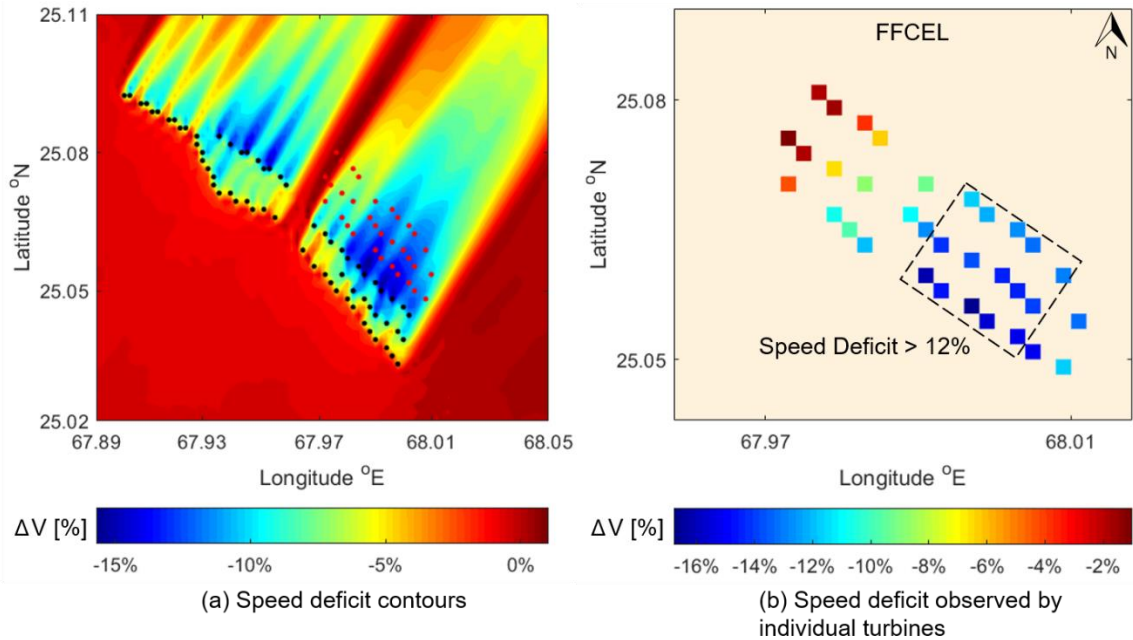
Figure 5.2 Speed deficit observed due to upstream wind farms wake

5.2   Power output characteristics

The power output characteristics of a wind farm are determined by a combination of different atmospheric and technical variables. In the current study, a constant air density of 1.225 kg m^{-3} was used and it was assumed that all the turbines are perfectly facing the prevailing wind direction. The power deficit observed by FFCEL due to the presence of

two upstream farms is displayed in Fig. 5.3. The values represented are averaged over five days of simulation. The power deficit showed high correspondence with the speed deficit results. Power loss greater than 22% can be observed in the turbines located on the South-East end, where some turbines experienced a substantial power deficit up to 35% as shown by the dotted rectangular box.
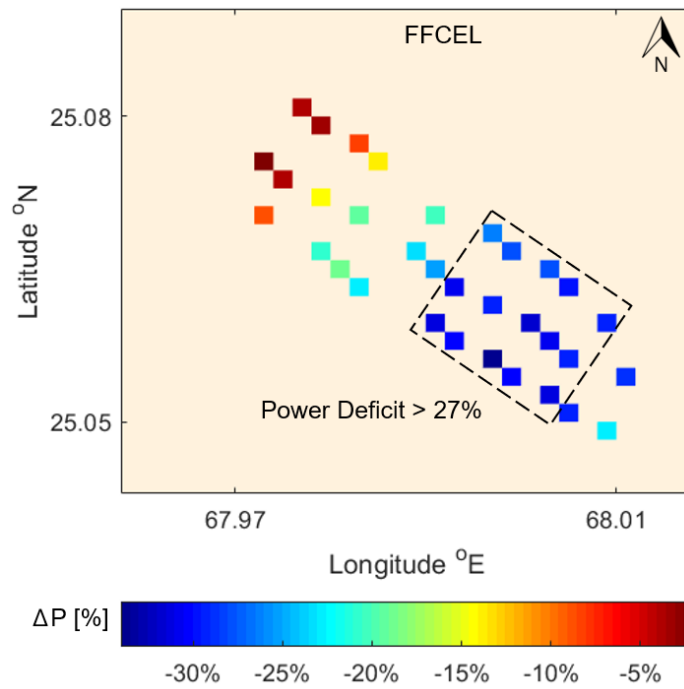
Figure 5.3 Wind turbines power deficit
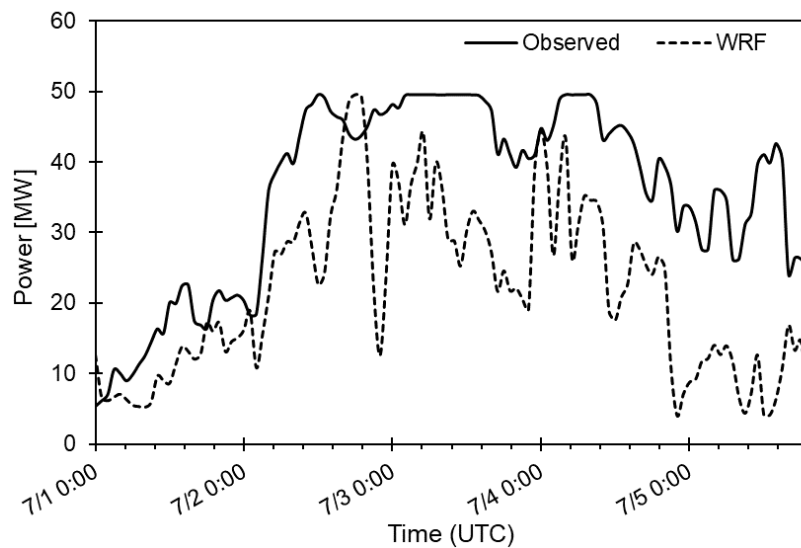
Figure 5.4 Wind farm total power output comparison between observed and WRF values

The temporal variation of total power produced by the FFCEL wind farm was also graphically analyzed with the observed power data obtained through SCADA loggers in Fig. 5.4. Underestimation caused by the WRF model in wind speeds prediction has translated into a further decline in total power generation, as turbine power is proportional to the cube of wind speed.

(a) Observed   (b) WRF
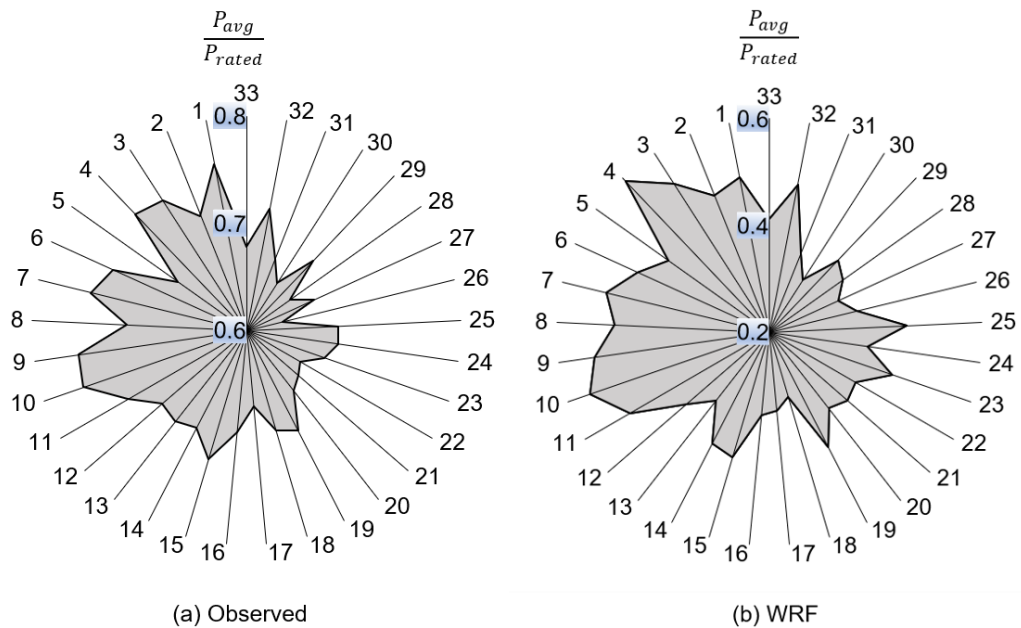
Figure 5.5 Normalized power of all turbines in FFCEL
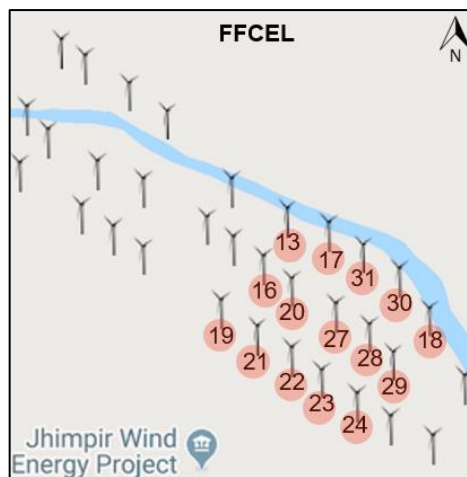
Figure 5.6 Selected turbines with the highest power deficit with their operational identification numbers

The normalized power output of all individual turbines in FFCEL was also investigated in Fig. 5.5 to identify the turbines most affected by upstream wind farms. The power output was normalized by Nordex S77 rated power i.e. 1500 kW. The vertical scales in Fig. are set at different lower and upper limits for the two data sets, to obtain a clear view of the power output trend followed by turbines. Turbines no 1 to 11 (See Fig. 3.4) are the most productive turbines on the farm. The highest power in both WRF and observed data can be seen in turbines no. 4, 9, and 10. These turbines are located at a relatively higher altitude and are outside the wake flow of upstream wind farms. Conversely, turbines situated on the South-East end, No. 16 to 31, displayed a significan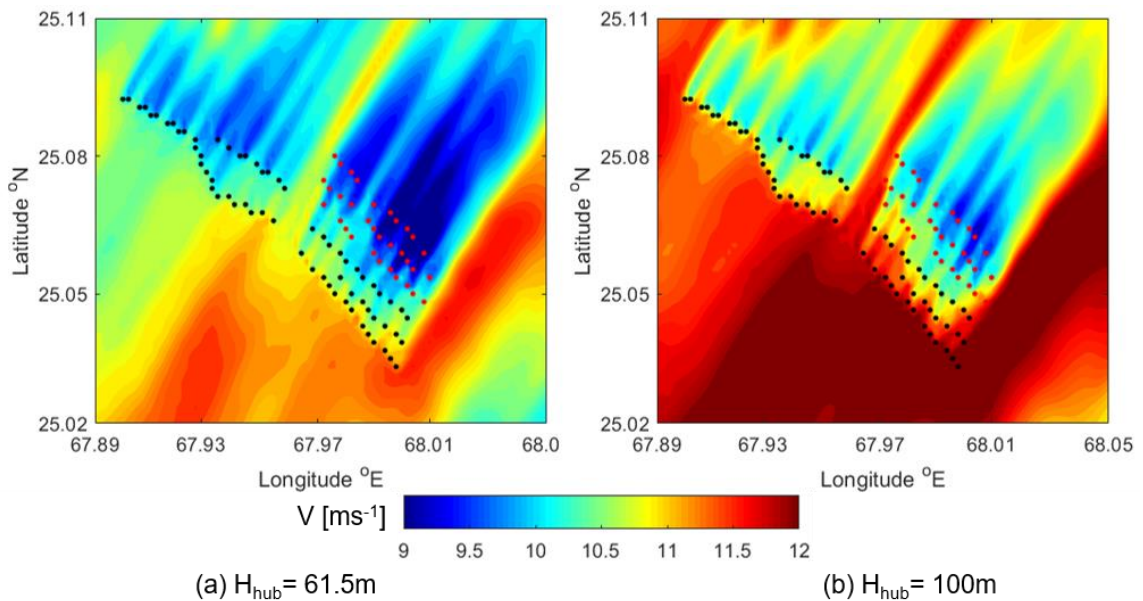t power drop due to wake effects. The turbines with the highest power deficit are also identified in Fig. 5.3 in a dotted rectangular box. These turbines are identified (Fig. 5.6) to undergo the partial repowering process to increase the overall power generation in FFCEL.

(a) H_{hub}= 61.5m   (b) H_{hub}= 100m

Figure 5.7 Velocity contours at the proposed hub heights of 61.5 m and 100 m

5.3   Hub height variation

In this section, a partial repowering strategy is discussed to augment the overall power production of the FFCEL wind farm. The hub heights of affected turbines (see Fig. 5.6) were varied to alleviate the wake effects. The available hub heights according to the standards provided by International Electrotechnical Commission (IEC) and German Institute for Construction Technology (DIBt) for Nordex S77 turbines are 61.5m, 80m,

85m, 90m, and 100m for cylindrical towers[41]. The hub heights of turbines identified in the previous section will be varied to 61.5m and 100m separately. The schematics of the proposed variation are displayed in Fig. 5.8 and the wind turbines upper and lower blade tips can be seen to change positions with respect to the wake flow.
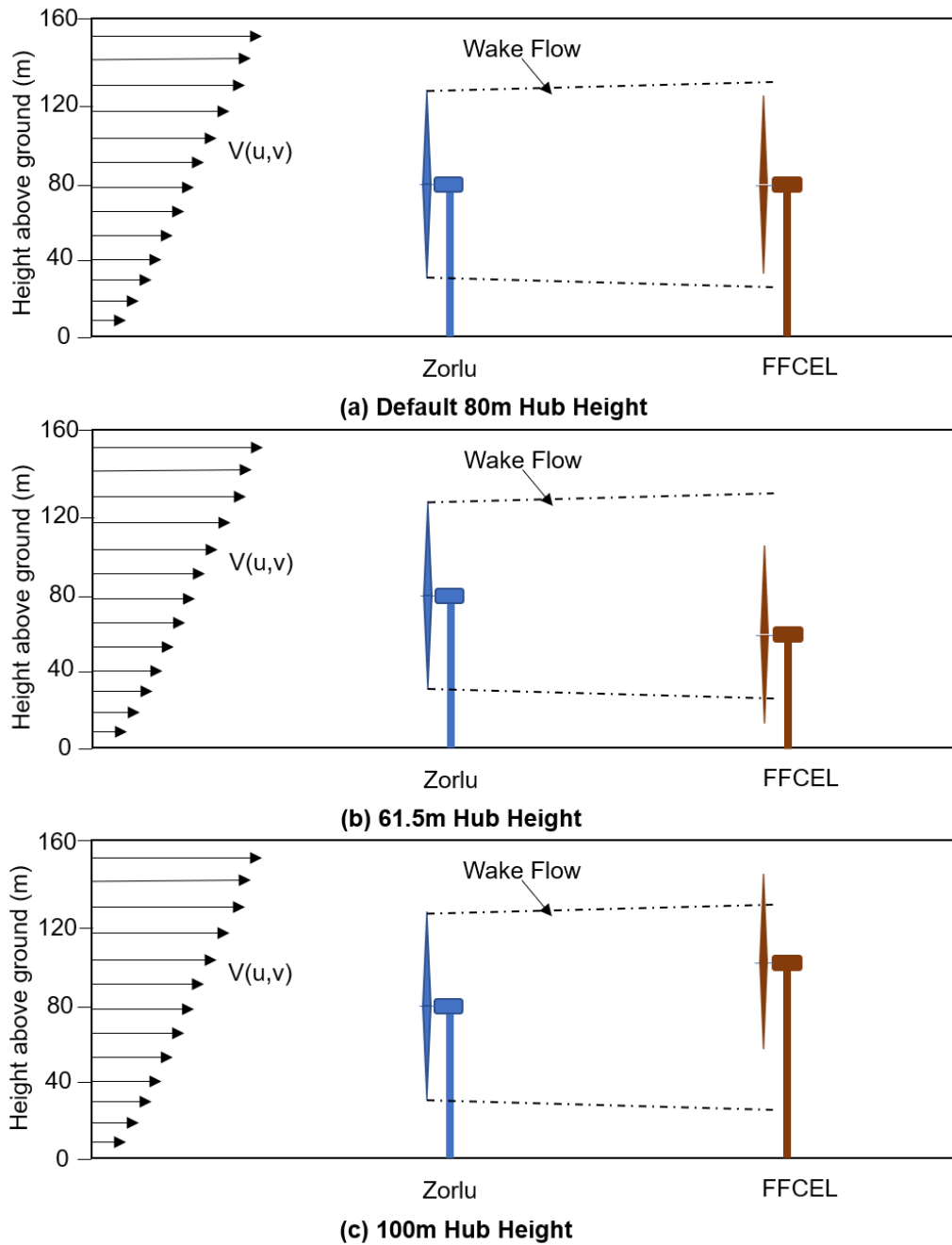
Figure 5.8 Proposed layout of selected turbines in FFCEL with 61.5m and 100m hub heights
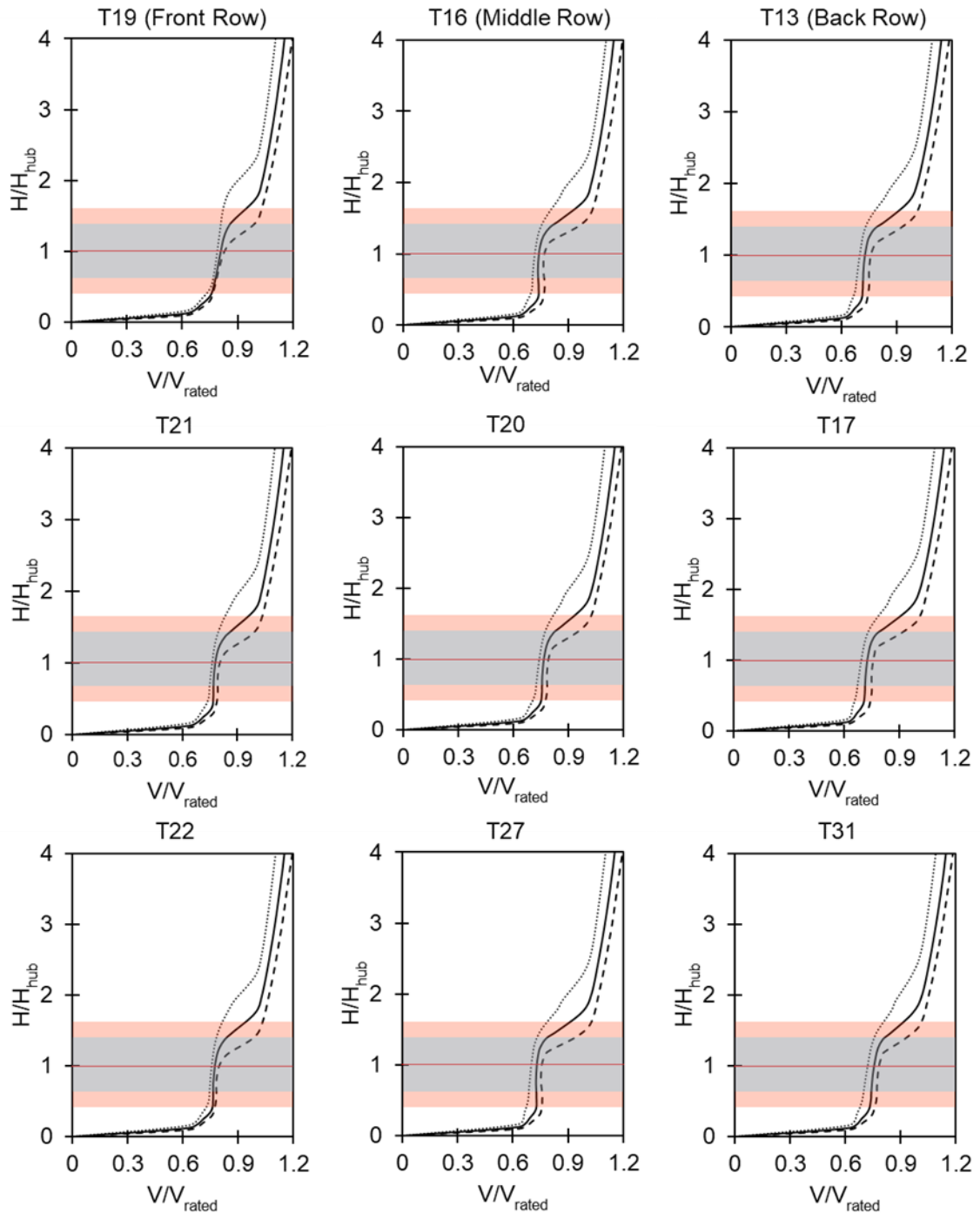
Figure 5.9 Wind shear profiles at H_{hub}=61.5m and H_{hub}=100m compared with H_{hub}=80m. Improved speed profiles are observed for H_{hub}=100m with a row-wise repetitive trend
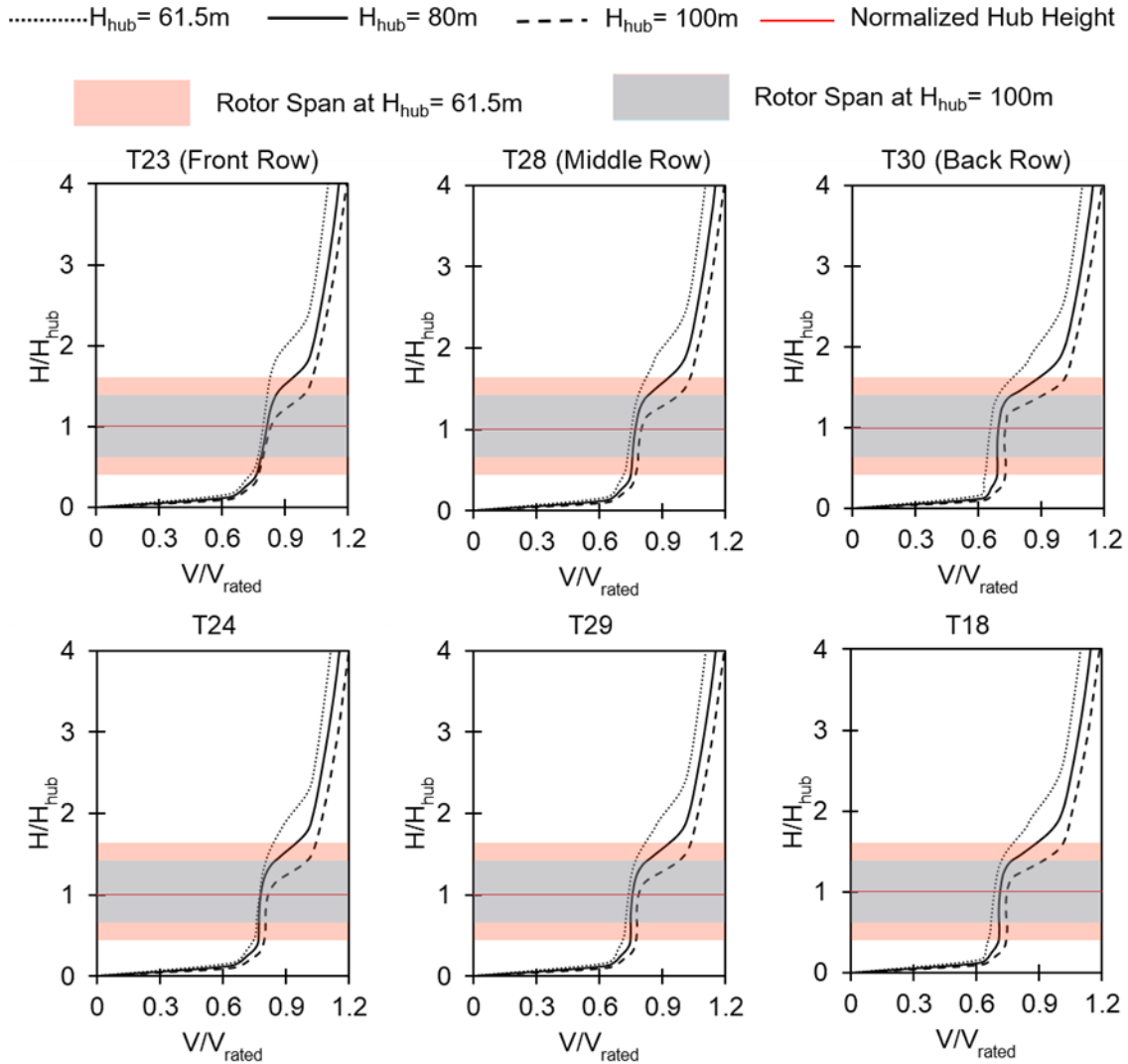
Figure 5.10 *(Continuation of Fig. 5.9)* Wind shear profiles at H_{hub}=61.5m and H_{hub}=100m compared with H_{hub}=80m. Improved speed profiles are observed for H_{hub}=100m with a row-wise repetitive trend

The speed contours obtained at the proposed hub heights are displayed in Fig. 5.7. An improvement in the speed observed by affected turbines can be seen for the H_{hub}=100m case, while a speed decline is experienced by the turbines in the H_{hub}=60m case.

The wind shear profiles are presented in Fig. 5.9 and Fig. 5.10 for all the affected turbines at existing and proposed hub heights. H/H_{hub} denotes the normalized height above ground, whereas V/V_{rated} is the normalized wind speed (where V_{rated}=12.5 ms^{-1}). A very mild change in wind speed profile was observed in the front row turbines (No. 19, 21, 22, 23, 24), as seen in the Fig., while a significant speed change is observed across the turbine

rotor for both H_{hub}=61.5m and H_{hub}=100m cases in the middle (No. 16, 20, 27, 28, 29) and back (No. 13, 17, 31, 30, 18) row turbines.

As observed from Fig. 5.9, varying the hub height of affected turbines to H_{hub}=61.5 m further decreased the incoming speed due to the increased shear as compared to the existing layout. The wind speed drop was observed both above and below the hub, although an increase was anticipated under the hub due to less wake interaction. An increased boundary layer shear near the ground also resulted in lower speeds at H_{hub}=61.5m. Conversely, a substantial gain in incoming wind speed was found for all the turbines at H_{hub}=100m across the turbine rotor due to decreased shear and wake interference.

The percentage of power variation in all the individual turbines in FFCEL can be observed in Fig. 5.11 for both cases. For H_{hub}=100m, the highest power gain was observed for back row turbines up to 13.6% compared to the existing layout. For the lower hub height case, the back-row turbines experienced the highest power reduction of up to 12.2%. The effect of hub height variation on all the unmodified turbines in the farm remained negligible.
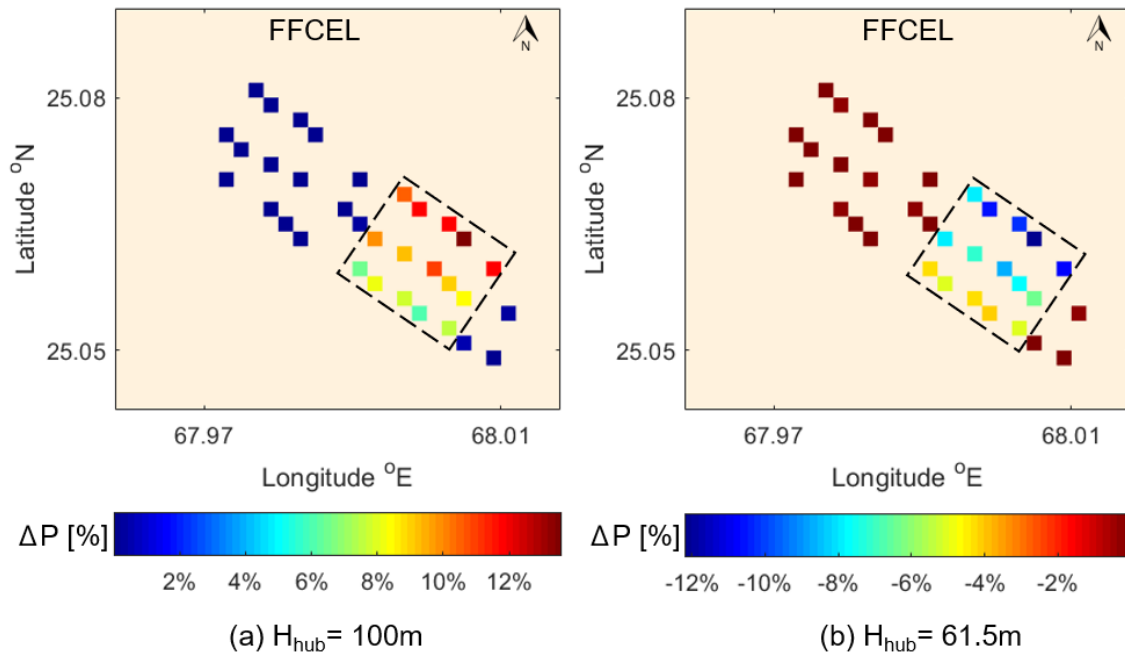
Figure 5.11 Power variation as a result of changing hub heights. Power improvement up to 13.6% is observed for H_{hub}=100m as compared to the existing layout
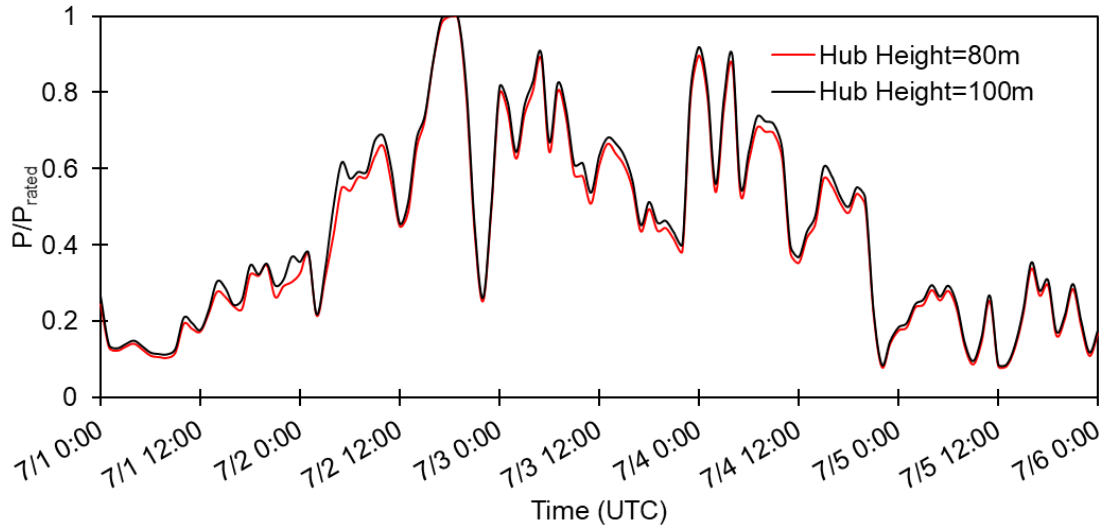
Figure 5.12 Temporal variation of total power generation in FFCEL for the proposed H_{hub}=100m and existing H_{hub}=80m. An average increase of 4.9% is observed for the modified layout.

The temporal variation of total power generation in FFCEL over the course of five days for H_{hub}=100m is compared with the existing layout in Fig. 5.12. An average increase of 4.9% was observed in the total power output when the hub height of selected turbines is modified to 100m in order to avoid the wake interference from upstream wind farms. Increasing the hub height of selected turbines presents an optimum partial repowering strategy for FFCEL which will significantly augment the annual energy production.

Summary

Wake interference results of upstream wind farms on FFCEL suggests a deficit of up to 15% in wind speed and up to 35% in power generation of individual turbines. Turbines located on the South-East side were more prone to wake losses due to terrain and layout characteristics. When the hub heights of selected turbines were varied to 61.5m and 100m, a further reduction was observed in the former case while an increase in power generation up to 13.6% was experienced in the latter case. An average increase of 4.9% in the total power generation of FFCEL was observed at the new hub heights of 100m.

Chapter 6

Conclusions

6.1 Conclusions

A partial repowering strategy was proposed for the FFCEL wind farm located in Jhimpir, Pakistan. The said farm is situated in complex terrain and is experiencing reduced power generation due to wake interference from the neighboring upstream wind farms. FFCEL is a packed wind farm with close intra-farm and inter-farm spacing, thus not allowing the wind speed to recover from wake effects. The wind farm parameterization scheme integrated with the mesoscale WRF model was applied to determine the speed and power reduction experienced by individual turbines. The model was run at a high horizontal resolution of 200m with five nested domains. A high resolution of geographical and time-dependent data was used to achieve higher accuracy. The model results were compared with the observed data obtained from a meteorological mast located in the vicinity of FFCEL.

1. Although WRF underestimated the wind speed, the model was satisfactorily validated with a mean absolute percentage error of only 14.7% and a high correlation coefficient of 0.72.

2. Technical data of wind turbines including the coordinates, power and thrust curves, were utilized to evaluate the wake interference between the three wind farms. A speed reduction of up to 16% was observed in the turbines on the South-East end of the farm due to higher wake interaction. A similar power trend was discovered with a reduction of up to 35 % in the wind turbine generators.

3. Power output in individual turbines was also calculated to identify the turbines with the worst performance under upstream farms wake interaction. The observed power data from the farm was also utilized for validation purposes. A group of fifteen turbines on the South-East end was identified for refurbishing purposes because of the highest power losses i.e. greater than 27%.

4. Hub heights of selected turbines were varied to 61.5m and 100m separately and the wind shear profiles, and power output data was analyzed and compared to the existing layout. It was noted that lowering the hub heights to H_{hub}=61.5m was not desirable as it further reduced the power generation due to increased shear. A considerable wind speed increase was found for H_{hub}=100m due to reduced wake interference and shear effects. The power output enhancement of up to 13.6% was observed in individual turbines. An average increase of 4.9% in the total power generation of FFCEL wind farms can lead to a significant increase in annual energy production.

6.2   Future Research Work

This research work has successfully presented a prospective repowering strategy for an inland wind farm influenced by upstream farms wake effects using the mesoscale model WRF. The outcomes of this study have opened many new avenues for exploration which are as follows:

a. Further validation of mesoscale models for wake analysis should be done using high fidelity models like CFD and LES which can resolve complex wake structures on a microscale level.

b. The performance of the Wind Farm Parameterization scheme should be evaluated on a variety of terrain and employing a range of different wind speeds and directions.

c. The results of this study need to be complemented by the economic aspects of repowering with the Annual Energy Production calculations.

d. An optimization study with the hub height variation of individual turbines can lead to a wind farm layout with even more power generation potential.

e. A fluid-structural analysis of modified turbines at H_{hub}=100m is imperative to observe the effects of fatigue on turbine blade regions that are now out of wake interaction.

f. As Pakistan is heading towards increased wind power capacity, a detailed repowering policy should be developed by all the stakeholders to augment the energy production from the established sites.

References

[1]   IRENA, "Renewable capacity statistics 2019, International Renewable Energy Agency (IRENA), Abu Dhabi," 2019.

[2]   B. Mendecka and L. Lombardi, "Life cycle environmental impacts of wind energy technologies: A review of simplified models and harmonization of the results," *Renew. Sustain. Energy Rev.*, vol. 111, no. April, pp. 462–480, 2019.

[3]   M. H. Baloch, G. S. Kaloi, and Z. A. Memon, "Current scenario of the wind energy in Pakistan challenges and future perspectives: A case study," *Energy Reports*, vol. 2, pp. 201–210, 2016.

[4]   M. F. Howland, S. K. Lele, and J. O. Dabiri, "Wind farm power optimization through wake steering," *Proc. Natl. Acad. Sci. U. S. A.*, vol. 116, no. 29, pp. 14495–14500, 2019.

[5]   C. L. Archer *et al.*, "Review and evaluation of wake loss models for wind energy applications," *Appl. Energy*, vol. 226, no. May 2018, pp. 1187–1207, 2018.

[6]   L. Wang, A. C. C. Tan, M. Cholette, and Y. Gu, "Comparison of the effectiveness of analytical wake models for wind farm with constant and variable hub heights," *Energy Convers. Manag.*, vol. 124, pp. 189–202, 2016.

[7]   S. Jeon, B. Kim, and J. Huh, "Comparison and verification of wake models in an onshore wind farm considering single wake condition of the 2 MW wind turbine," *Energy*, vol. 93, pp. 1769–1777, 2015.

[8]   X. Gao, H. Yang, and L. Lu, "Optimization of wind turbine layout position in a wind farm using a newly-developed two-dimensional wake model," *Appl. Energy*, vol. 174, pp. 192–200, 2016.

[9]   N. O. Jensen, "A note on wind generator interaction," *Risø-M-2411 Risø Natl. Lab. Roskilde*, pp. 1–16, 1983.

[10]   I. Katic, J. Hojstrup, and N. O. Jensen, "A simple model for cluster efficiency i.katic. j.højstrup. n.o.jensen," *Eur. Wind energy Assoc. Conf. Exhib. 1986*, no.

October, pp. 407–410, 1986.

[11]   S. Frandsen *et al.*, "Analytical modelling of wind speed deficit in large offshore wind farms," *Wind Energy*, vol. 9, no. 1–2, pp. 39–53, 2006.

[12]   H. Sun and H. Yang, "Study on an innovative three-dimensional wind turbine wake model," *Appl. Energy*, vol. 226, no. May, pp. 483–493, 2018.

[13]   Y. Wang, W. Miao, Q. Ding, C. Li, and B. Xiang, "Numerical investigations on control strategies of wake deviation for large wind turbines in an offshore wind farm," *Ocean Eng.*, vol. 173, no. December 2018, pp. 794–801, 2019.

[14]   F. Porté-Agel, Y. T. Wu, H. Lu, and R. J. Conzemius, "Large-eddy simulation of atmospheric boundary layer flow through wind turbines and wind farms," *J. Wind Eng. Ind. Aerodyn.*, vol. 99, no. 4, pp. 154–168, 2011.

[15]   X. Yang, M. Pakula, and F. Sotiropoulos, "Large-eddy simulation of a utility-scale wind farm in complex terrain," *Appl. Energy*, vol. 229, no. May, pp. 767–777, 2018.

[16]   Y. T. Wu, T. L. Liao, C. K. Chen, C. Y. Lin, and P. W. Chen, "Power output efficiency in large wind farms with different hub heights and configurations," *Renew. Energy*, vol. 132, pp. 941–949, 2019.

[17]   G. P. Navarro Diaz, A. C. Saulo, and A. D. Otero, "Wind farm interference and terrain interaction simulation by means of an adaptive actuator disc," *J. Wind Eng. Ind. Aerodyn.*, vol. 186, no. September 2018, pp. 58–67, 2019.

[18]   S. Naderi, S. Parvanehmasiha, and F. Torabi, "Modeling of horizontal axis wind turbine wakes in Horns Rev offshore wind farm using an improved actuator disc model coupled with computational fluid dynamic," *Energy Convers. Manag.*, vol. 171, no. May, pp. 953–968, 2018.

[19]   J. Kuo, D. Rehman, D. A. Romero, and C. H. Amon, "A novel wake model for wind farm design on complex terrains," *J. Wind Eng. Ind. Aerodyn.*, vol. 174, no. January, pp. 94–102, 2018.

[20] Z. Guo and X. Xiao, "Wind power assessment based on a WRF wind simulation with developed power curve modeling methods," *Abstr. Appl. Anal.*, vol. 2014, 2014.

[21] E. M. Giannakopoulou and R. Nhili, "WRF model methodology for offshore wind energy applications," *Adv. Meteorol.*, vol. 2014, 2014.

[22] A. C. Fitch *et al.*, "Local and mesoscale impacts of wind farms as parameterized in a mesoscale NWP model," *Mon. Weather Rev.*, vol. 140, no. 9, pp. 3017–3038, 2012.

[23] P. A. Jiménez, J. Navarro, A. M. Palomares, and J. Dudhia, "Mesoscale modeling of offshore wind turbine wakes at the wind farm resolving scale: a composite-based analysis with the Weather Research and Forecasting model over Horns Rev," *Wind Energy*, vol. 18, no. 3, pp. 559–566, Mar. 2015.

[24] R. Yuan *et al.*, "Coupled wind farm parameterization with a mesoscale model for simulations of an onshore wind farm," *Appl. Energy*, vol. 206, no. August, pp. 113–125, 2017.

[25] Q. Wang, K. Luo, R. Yuan, S. Zhang, and J. Fan, "Wake and performance interference between adjacent wind farms: Case study of Xinjiang in China by means of mesoscale simulations," *Energy*, vol. 166, pp. 1168–1180, 2019.

[26] J. C. Y. Lee and J. K. Lundquist, "Evaluation of the wind farm parameterization in the Weather Research and Forecasting model (version 3.8.1) with meteorological and turbine power data," *Geosci. Model Dev.*, vol. 10, no. 11, pp. 4229–4244, 2017.

[27] R. J. Mangara, Z. Guo, and S. Li, "Performance of the Wind Farm Parameterization Scheme Coupled with the Weather Research and Forecasting Model under Multiple Resolution Regimes for Simulating an Onshore Wind Farm," *Adv. Atmos. Sci.*, vol. 36, no. 2, pp. 119–132, 2019.

[28] F. Porté-agel, M. Bastankhah, and S. Shamsoddin, *Wind-Turbine and Wind-Farm Flows : A Review*. Springer Netherlands, 2019.

[29]   Y. Chen, H. Li, K. Jin, and Q. Song, "Wind farm layout optimization using genetic algorithm with different hub height wind turbines," *Energy Convers. Manag.*, vol. 70, pp. 56–65, 2013.

[30]   K. Chen, M. X. Song, X. Zhang, and S. F. Wang, "Wind turbine layout optimization with multiple hub height wind turbines using greedy algorithm," *Renew. Energy*, vol. 96, pp. 676–686, 2016.

[31]   A. Vasel-Be-Hagh and C. L. Archer, "Wind farm hub height optimization," *Appl. Energy*, vol. 195, pp. 905–921, 2017.

[32]   S. Baidya Roy, S. W. Pacala, and R. L. Walko, "Can large wind farms affect local meteorology?," *J. Geophys. Res. D Atmos.*, vol. 109, no. 19, pp. 1–6, 2004.

[33]   S. Baidya Roy, "Simulating impacts of wind farms on local hydrometeorology," *J. Wind Eng. Ind. Aerodyn.*, vol. 99, no. 4, pp. 491–498, 2011.

[34]   U. Blahak, B. Goretzki, and J. Meis, "A simple parameterization of drag forces induced by large wind farms for numerical weather prediction models," *Eur. Wind Energy Conf. Exhib. 2010, EWEC 2010*, vol. 6, no. 1, pp. 4577–4585, 2010.

[35]   W. C. Skamarock *et al.*, "A Description of the Advanced Research WRF Model Version 4 NCAR Technical Note," *Natl. Cent. Atmos. Res.*, p. 145, 2019.

[36]   R. Laprise, "The Euler equations of motion with hydrostatic pressure as an independent variable," *Monthly Weather Review*, vol. 120, no. 1. pp. 197–207, 1991.

[37]   M. Nakanishi and H. Niino, "Development of an improved turbulence closure model for the atmospheric boundary layer," *J. Meteorol. Soc. Japan*, vol. 87, no. 5, pp. 895–912, 2009.

[38]   Hong, S.–Y., and J.–O. J. Lim, 2006: The WRF single–moment 6–class microphysics scheme (WSM6). J. Korean Meteor. Soc., 42, 129–151.

[39]   G. A. Grell and S. R. Freitas, "A scale and aerosol aware stochastic convective parameterization for weather and air quality modeling," *Atmos. Chem. Phys.*, vol.

14, no. 10, pp. 5233–5250, 2014.

[40]   K. Mohammadi, O. Alavi, A. Mostafaeipour, N. Goudarzi, and M. Jalilvand, "Assessing different parameters estimation methods of Weibull distribution to compute wind power density," *Energy Convers. Manag.*, vol. 108, pp. 322–335, 2016.

[41]   Nordex S77 / 1500 kW Turbine (2005) Facts and Figures. Accessed on: May 30, 2019. [Online]. Available: http://www.nordex-online.com/fileadmin/MEDIA/Produktinfos/EN/Nordex_S70_S77_Produktbrosch uere_EN.pdf

Appendix A: WRF Preprocessing System Domains

WPS Domain Configuration
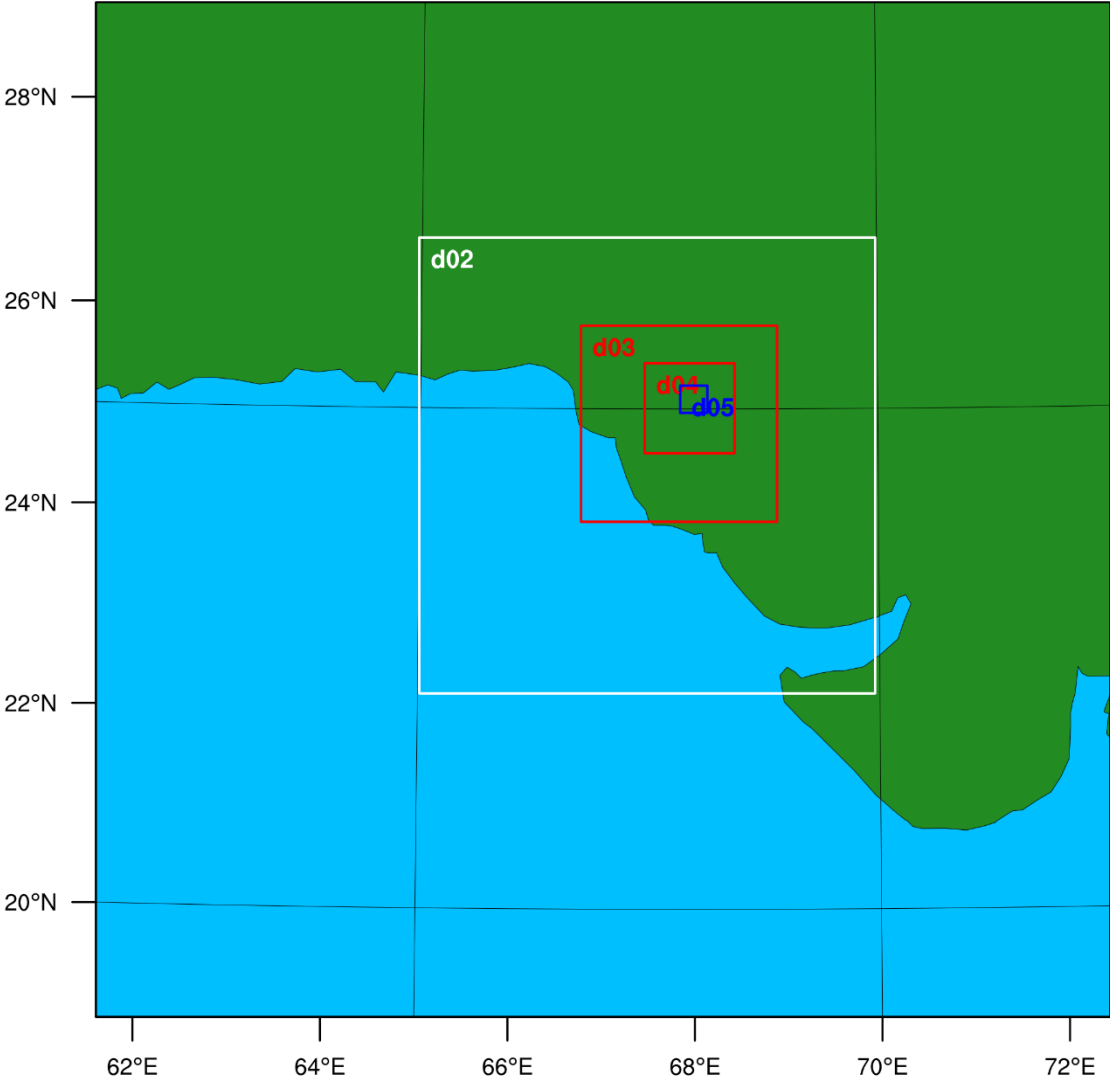
Appendix B: NCAR Command Language (NCL) code for postprocessing WRF output

```
load "$NCARG_ROOT/lib/ncarg/nclscripts/csm/gsn_code.ncl"
load "$NCARG_ROOT/lib/ncarg/nclscripts/wrf/WRFUserARW.ncl"
begin
  a = addfile("./wrfout_d05_2018-07-01_00:00:00","r")
; Plot type
; type = "x11"
  type = "pdf"
  wks = gsn_open_wks(type,"some_times")
  res = True    ; Set some basic resources
  res@InitTime    = False
  res@MainTitle = "REAL-TIME WRF"
  res@Footer = False
  pltres = True
  mpres = True
  mpres@mpGeophysicalLineColor = "Black"
  mpres@mpNationalLineColor    = "Black"
  mpres@mpUSStateLineColor     = "Black"
  mpres@mpGridLineColor        = "Black"
  mpres@mpLimbLineColor        = "Black"
  mpres@mpPerimLineColor       = "Black"
; What times and how many time steps are in the data set?
  times = wrf_user_getvar(a,"times",-1)  ; get all times in the file
  ntimes = dimsizes(times)       ; number of times in the file
  lats = (/  25.026,  25.116 /)
  lons = (/ 67.893, 68.054 /)
  loc = wrf_user_ll_to_ij(a, lons, lats, True)
; loc(0,;) is west-east (x) ; loc(1,:) is south-north (y)
; subtract one since we want to use it as an index in NCL
```

```
 x_start = loc(0,0) - 1
 x_end   = loc(0,1) - 1
 y_start = loc(1,0) - 1
 y_end   = loc(1,1) - 1
pos=wrf_user_ij_to_ll(a, x_end+1, y_end+1, True)
print("end lon is: "+pos(0))
print("end lat is: "+pos(1))
 mpres@ZoomIn = True        ; set up map info for zoomed area
 mpres@Xstart = x_start
 mpres@Ystart = y_start
 mpres@Xend = x_end
 mpres@Yend = y_end
print("y start is:  "+y_start)
print("y end is   :  "+y_end)
print("x start is:  "+x_start)
print("x end is   :  "+x_end)
do it = 0, ntimes-1            ; TIME LOOP
    print("Working on time: " + times(it) )
    res@TimeLabel = times(it)   ; Set Valid time to use on plots
    tc = wrf_user_getvar(a,"tc",it)         ; T in C
    uvm = wrf_user_getvar(a,"uvmet",it)
    u = uvm(0,:,:,:)
    v = uvm(1,:,:,:)
    z  = wrf_user_getvar(a, "z",it)         ; grid point height
    ter = wrf_user_getvar(a, "ter",it) ; model terrain height
; Conform data to Terrain Height
   nheight = conform(z,ter,(/1,2/))
   z = z - nheight
      u_plane  = wrf_user_intrp3d( u,z,"h",100,0.,False)
      u_plane_zoom = u_plane(y_start:y_end,x_start:x_end)
; create a zoomed area
```

```
     v_plane   = wrf_user_intrp3d( v,z,"h",100,0.,False)

     v_plane_zoom = v_plane(y_start:y_end,x_start:x_end)

     u_plane@units = "m/s"

     v_plane@units = "m/s"

     ; Calculate Wind Speed from Vectors

     spd = (u_plane*u_plane + v_plane*v_plane)^(0.5)

     spd_zoom = spd(y_start:y_end,x_start:x_end)

     spd@description = "Wind Speed"

     spd@units = "m/s"

   ; Plotting options for Wind Vectors

     opts = res

     opts@FieldTitle = "Wind"    ; overwrite Field Title

     opts@vcGlyphStyle = "LineArrow"

     opts@NumVectors = 47        ; wind barb density

     vector = wrf_vector(a,wks,u_plane_zoom,v_plane_zoom,opts)

     delete(opts)

     opts = res

     opts@cnFillOn = True

     opts@ContourParameters = (/ 7., 14., 0.1/)

     opts@cnFillOn           = True

     contour_spd = wrf_contour(a,wks,spd_zoom,opts)

     delete(opts)

   ; MAKE PLOTS

   plot = wrf_map_overlays(a,wks,(/contour_spd/),pltres,mpres)

 asciiwrite("allthreehubhundered.txt",spd_zoom)

end do        ; END OF TIME LOOP


end
```

Notes